International Journal of Nanomedicine

Dovepress
Taylor & Francis Group

Open Access Full Text Article

ORIGINAL RESEARCH

Phytosomes Loaded with Mastoparan-M Represent a Novel Strategy for Breast Cancer Treatment

Hairong Zhao[1,2,*], Shuangyan Bao[2,*], Shuanglong Chen[1,*], Qingmo Yang[1,*], Kangliang Lou[3], Yating Gai[4], Jinyan Lin[5], Chaojie Liu[2], Heng Liu[2], Chenggui Zhang[2], Ruiqin Yang[1]

[1]Department of Breast Surgery, The First Affiliated Hospital of Xiamen University, School of Medicine, Xiamen University, Xiamen, People's Republic of China; [2]Yunnan Provincial Key Laboratory of Entomological Biopharmaceutical R&D, Dali University, Dali, People's Republic of China; [3]School of Medicine, Xiamen University, Xiamen, People's Republic of China; [4]Xiamen Research Institute of Food and Drug Quality Inspection, Xiamen, People's Republic of China; [5]School of Public Health, Xi'an Jiaotong University, Xi'an, People's Republic of China

*These authors contributed equally to this work

Correspondence: Ruiqin Yang, Department of Breast Surgery, the First Affiliated Hospital of Xiamen University, School of Medicine, Xiamen University, Xiamen, People's Republic of China, Email yrqxm0822@163.com; Chenggui Zhang, Yunnan Provincial Key Laboratory of Entomological Biopharmaceutical R&D, Dali University, Dali, People's Republic of China, Email chenggui_zcg@163.com

Purpose: Mastoparan-M (Mast-M) has cytotoxic effects on various tumor cells in vitro, including liver cancer and colorectal cancer. However, the anti-tumor mechanism of Mast-M remains unclear and its potential for anti-tumor therapy has not been investigated. Herein, we aimed to develop a novel phytosome formulation loaded with Mast-M and evaluate its efficacy against breast cancer both in vitro and in vivo. Furthermore, we investigated the underlying anti-tumor mechanisms of Mast-M.

Methods: The synthesis of Phy-Mast-M involved a co-solvent technique, followed by solvent evaporation. Its anti-tumor mechanism was investigated using CCK-8, clone formation, and apoptosis assays. Subsequently, the biodistribution and anti-tumor efficacy of Phy-Mast-M were assessed in vivo using the 4T1 tumor-bearing mouse model. Finally, the safety of Phy-Mast-M was evaluated in vivo.

Results: The prepared Phy-Mast-M demonstrated an exceptional monodisperse size distribution (125.67 ± 45.79 nm), and exhibited excellent stability under different physiological conditions. Phy-Mast-M could inhibit 4T1 cells growth through multiple channels, including arresting cell growth cycle and disturbing mitochondrial membrane integrity. Phy-Mast-M proved significantly higher accumulation at tumor sites in a tumor-bearing mouse model as compared to free Mast-M. Moreover, in vivo anti-tumor studies demonstrated that Phy-Mast-M exhibited superior curative inhibitory effects on tumor growth and favorable biocompatibility.

Conclusion: Phy-Mast-M demonstrates significant anti-tumor activity both in vitro and in vivo. Moreover, its potential for clinical translation suggests promising prospects for cancer therapy, offering more drug options for breast cancer patients.

Keywords: breast cancer, Mast-M, phytosomes, cancer therapy, small molecule peptide

Introduction

Breast cancer is the most commonly diagnosed cancer and the leading cause of cancer-related deaths in women.[1] Currently, systemic chemotherapy remains a primary treatment option for breast cancer, especially for triple-negative breast cancer, due to a lack of precise therapeutic targets.[2,3] However, nearly half of all cancer patients experience treatment failure because of drug resistance or non-responsiveness to therapeutic drugs.[4,5] Therefore, there is an urgent need to develop new anti-tumor drugs with high efficiency and low toxicity for systemic breast cancer treatment.[6]

Venom therapy, regarded as a complementary and alternative medicine approach, has been used for centuries in folk medicine to treat pain, inflammation, and arthritis. *Vespa magnifica* (Smith) is a species of social wasp indigenous to Yunnan, China. Compounds extracted from wasp venom have been used clinically as anti-inflammatory medicines to

Received: 7 June 2024
Accepted: 5 December 2024
Published: 9 January 2025

Graphical Abstract

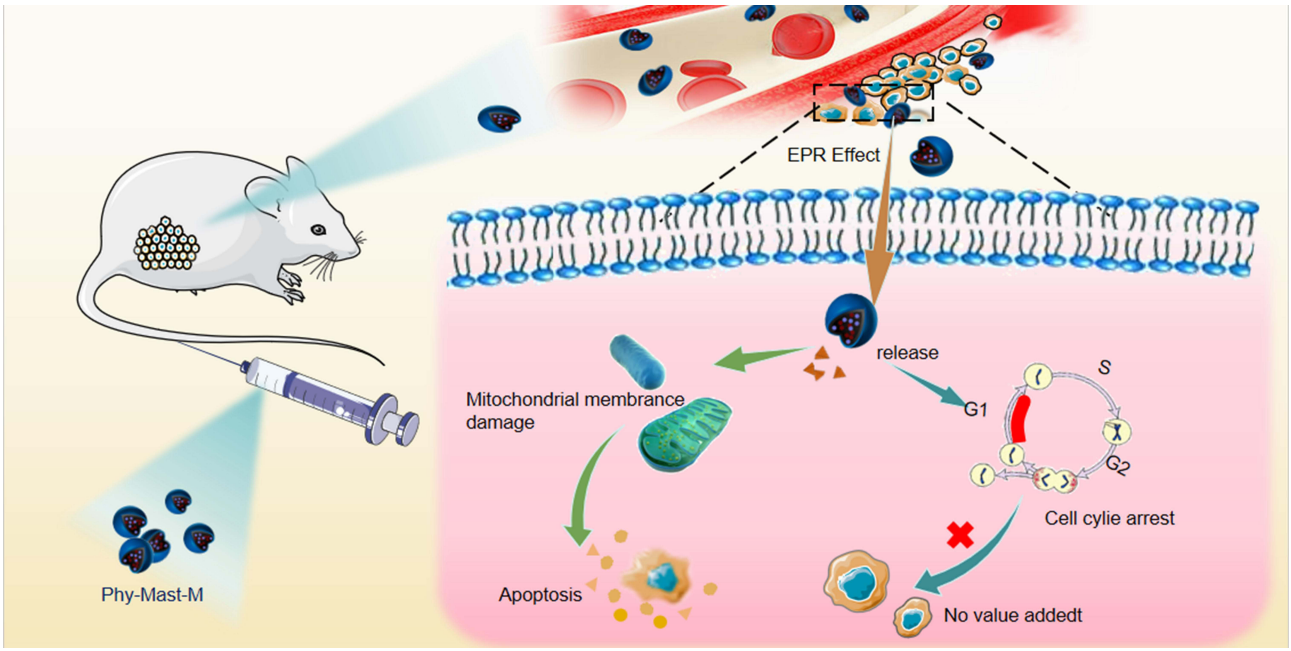

relieve pain and manage chronic inflammatory diseases, such as rheumatoid arthritis and multiple sclerosis.[7–9] Furthermore, Mast-M is an active component of tetradecapeptide, which our team isolated and identified from Yunnan Dehong *Vespa magnifica*. It constitutes 70–80% of the crude toxin extract.[10,11] Our previous studies have confirmed that Mast-M has neuroprotective, anti-inflammatory, and paw swelling-alleviating effects in rats with rheumatoid arthritis.[12,13] Interestingly, we have found that Mast-M has cytotoxic effects in vitro, including on various tumor cell types (liver cancer and melanoma cells).[10] Consequently, we posit that Mast-M peptide holds promise as a novel anti-tumor active ingredient, offering fresh insights for the development of new anti-cancer therapeutics. Nevertheless, the precise mechanism by which Mast-M peptide exerts its tumoricidal effects remains unclear, and further investigation into its in vivo anti-tumor efficacy is warranted.

As an ideal anti-tumor agent exhibit characteristic including safety, high efficacy, and multi-target selectivity. However, due to its inherent nature as a small molecule peptide, Mast-M is subject to rapid metabolism and exhibits a brief circulation time in the bloodstream. This poses challenges for achieving effective accumulation at tumor sites.[13–15] These characteristics constrain the application of Mast-M in cancer therapy. Modifying the delivery method to change the biodistribution of therapeutics has become a primary strategy. Research on nanomedicines is rapidly expanding, particularly regarding liposomes, which are favored for their biomimetic properties as nanoparticles composed of concentric self-assembled lipid bilayers. These structures exhibit prolonged circulation times in the bloodstream and can accumulate at tumor sites due to the enhanced permeability and retention (EPR) effect.[16–18] Furthermore, nanoformulations incorporating chemotherapeutic agents such as paclitaxel within liposomes are widely utilized for treating solid tumors and malignant hematologic conditions like breast cancer.[19] Moreover, in contrast to conventional liposomes, phytosomes—formed from complexes of phospholipids and active substances—demonstrate superior drug-loading capacity and sustained release profiles.[20] We hypothesize that Mast-M may interact with phospholipids through multiple weak interactions to form a Mast-M-phospholipid complex, thereby facilitating the development of Mast-M via self-assembly. This approach is intended to enhance both bioavailability and therapeutic efficacy of Mast-M.

In the current investigation, we have developed Phy-Mast-M, an innovative drug formulation that employs Mast-M as the active agent against tumors and utilizes phytosomes as drug delivery vehicles. Our strategy is designed to preserve

the pharmacological efficacy of Mast-M while optimizing its biodistribution and circulation time to enhance its antitumor effectiveness. Furthermore, it is imperative to investigate the mechanisms underlying its tumor growth inhibition. This research will provide substantial value and serve as a reference for the development of novel anticancer therapeutics.

Methods

Animal Preparation

Female BALB/c mice aged 6–8 weeks were purchased from Guangdong Yaokang Biological Technology Co. Ltd. All animal work was approved by the Institutional Ethical Committee of Animal Experimentation at Xiamen University (Ethics Approval: No. XMU\u0002LAC20180037) and was conducted in accordance with the principles of the Association for Assessment and Accreditation of Laboratory Animal Care International (AAALAC).

Cell Culture

All cancer cells were procured from the American Type Culture Collection in Rockville, USA. MCF-10A, the normal breast epithelial cell line were obtained from Procell Life Science & Technology Co., Ltd. (Wuhan, China), and were cultured in specific epithelial culture medium (CL-0525, Procell Co., Ltd). 4T1 and BT-549 cell lines were maintained in RPMI-1640 medium (Thermo Fisher) supplemented with 10% fetal bovine serum (FBS; Cellmax, China) and 1% penicillin-streptomycin. MDA-MB-231, Hela, CT-26, HepG2 and HT-29 cell lines were maintained in Dulbecco's Modified Eagle Medium (DMEM; Thermo Fisher) supplemented with 10% FBS and 1% penicillin-streptomycin. All cells were cultured in a standard humidified cell culture incubator (37°C, 5% CO_2).

Phy-Mast-M Synthesis

Mast-M (10 mg) and soya phosphatidylcholines (SPC) (30 mg) were dissolved in anhydrous ethanol (10 mL) and stirred continuously at 45°C for 4 h. The resulting mixture was subjected to spin steaming at 50°C to remove the reaction solvent. This was followed by the addition of 10 mL of ultra-pure water for ultrasonic hydration. Subsequently, any remaining free Mast-M and SPC were removed by dialysis in ultra-pure water containing 5% Tween 80. The mixture was sequentially extruded through 100 nm and 200 nm polycarbonate membranes for at least 15 cycles using an Avanti mini extruder to synthesize Phy-Mast-M. It was then stored in a refrigerator at 4°C for subsequent use. Next, Mast-M was labeled with fluorescein isothiocyanate (FITC) at a mass ratio of 1:1 (FITC 10 mg, Mast-M 10 mg), dissolved in 1mL DMSO, stirred overnight, and then mixed with 10 mL ultra-pure water to form FITC-Mast-M. To prepare FITC-Phy-Mast-M, Phy-Mast-M could be synthesized by incorporating FITC-labeled Mast-M during the synthesis process. Furthermore, Mast-M-ICG was synthesized by Shanghai Apeptide Company, Ltd. (Shanghai, China).

The capacity of Mast-M in Phy-Mast-M was determined utilizing high-performance liquid chromatography (HPLC) with an Agilent C18 analytical column, and detection was performed at a wavelength of 220 nm. The mobile phase consisted of acetonitrile and 0.1% trifluoroacetic acid (TFA). The flow rate was maintained at 1 mL/min, and the analytic volume was 10 μL. To confirm the successful binding of Mast-M with SPC, Fourier-transform infrared spectroscopy (FTIR) was employed to analyze SPC, Mast-M, and Phy-Mast-M. Given the insolubility of Mast-M in dichloromethane, the interaction between Mast-M and SPC was investigated by observing the dissolution behavior of Mast-M in dichloromethane. Mast-M, SPC, SPC+Mast-M, and Phy-Mast-M were dissolved in dichloromethane separately to observe dissolution behavior.

Characterization of Phy-Mast-M

General Properties of Drug Particles

Phy-Mast-M were prepared and subsequently diluted tenfold with phosphate-buffered saline (PBS). Following dilution, rigorous assessments were conducted to evaluate the color, clarity, and transparency of the solution.

TEM, Size, and Zeta Potential Analysis of Phy-Mast-M

The morphology and diameter distribution of Phy-Mast-M were assessed while it was dispersed on a carbon-coated copper grid using TEM (Thermo Fisher Scientific, Waltham, Massachusetts, USA). The particle size and zeta potential of Phy-Mast-M were measured with a Malvern Laser Particle Size Analyzer (Zetasizer Nano ZS 90, Malvern, UK) at 25°C.

Stability of Phy-Mast-M

In order to test the stability of Phy-Mast-M, a series of experiments were conducted. First, Phy-Mast-M was diluted tenfold and allowed to stand for 0, 6, 12, 24, and 48 h to observe the presence of any precipitate or flocculent formations. Subsequently, the dispersion quality was evaluated after 48 h placement using laser irradiation. Furthermore, the stability of Phy-Mast-M was investigated in various media such as PBS, 10% FBS, water, and DMEM cell culture medium. Hydrodynamic diameters of the solutions were measured at 0, 6, 12, 24, and 48 h. Finally, the stability of Phy-Mast-M was analyzed using HPLC to quantify the Mast-M content in Phy-Mast-M samples stored for 0, 7, 14, and 28 days.

Cytotoxicity Assay

MDA-MB-231, 4T1, BT-549, Hela, CT-26, HepG2, HT-29 and MCF-10A cells (1×10^4 cells/well) were seeded in 96-well plates for an initial 12 h incubation. The medium was then replaced with fresh culture medium containing different concentrations of Mast-M and Phy-Mast-M. Following another 24 h incubation, the cell viability was determined using the CCK-8 assay kit provided by Beyotime Biotechnology.

Cellular Uptake and Colocalization

The internalization of Phy-Mast-M was evaluated by a confocal microscopic examination following the co-culturing of FITC-Phy-Mast-M and FITC-Mast-M with 4T1 cells. Specifically, 4T1 cells (1×10^5 cells/well) were seeded in 12-well plates and incubated for 12 h. Subsequently, the cell culture medium was replaced with fresh media containing FITC-Phy -Mast-M and FITC-Mast-M (equivalent in Mast-M content) for an additional 1, 3, and 6 h of incubation. Following incubation, 4T1 cells were rinsed twice with PBS and fixed with 4% formaldehyde for 15 min at room temperature. To visualize the cellular uptake of Phy-Mast-M, the cell nuclei were first counterstained with DAPI, and the cell membranes with Dil, both procured from Beyotime Biotechnology, in accordance with the supplier's standard operating procedures. Following this, coverslips were mounted onto glass slides using an anti-fade reagent from Beyotime Biotechnology to preserve fluorescence integrity. The samples were then examined using the Leica DM2700 Portho fluorescence microscope (Leica Microsystems, Wetzlar, Germany).

Annexin V-FITC/PI Apoptosis Detection

4T1 cells (2×10^5 cells/well) were plated in a 6-well plate for an initial 12 h incubation. They were then treated with Mast-M or Phy-Mast-M and further incubated for 24 h. Subsequently, cells were washed twice and treated with 50 μL of 1× binding buffer, suspended, and transferred into a 2 mL centrifuge tube. Then, 2.5 μL FITC Annexin V and 2.5 μL PI (Beyotime Biotechnology) was added, vortex cells were incubated at room temperature for 15 min away from light. Finally, 450 μL of 1× binding buffer was added into each tube and the tubes were analyzed via flow cytometry (CytoFlexS) within 1 h.

Western Blot

The total protein was separated by RIPA lysis buffer with 1 mm PMSF (HY-L081 Med Chem Express, USA) and protease inhibitor cocktail (HY-K0010 Med Chem Express, USA) for 15 min, followed by 15 min centrifugation at 12000 rpm at 4°C. Protein concentration was measured using BCA protein assay kit (P0011, Beyotime, China). Protein was separated with SDS-polyacrylamide gel electrophoresis, and then transferred from the gel onto a polyvinylidene difluoride (ISEQ00010, Millipore, USA) membrane. After being blocked with 5% nonfat dry milk in Tris-buffered saline plus Tween-20 (TBST) for 1.5 h at room temperature, the PVDF membranes were incubated with primary antibodies overnight at 4°C, and then with secondary antibodies for 1 h at room temperature. The membranes were washed with TBST buffer, the blots were visualized by Azure C300. The information of antibodies is as follows: Caspase-3 (1:1000, 14220, Cell Signaling Technology, USA). Bax (1:1000, 5023, Cell Signaling Technology, USA).

Mitochondrial Membrane Detection

Mitochondrial membranes of 4T1 cells were evaluated by confocal microscopic observation after culturing the Phy-Mast -M and vector with 4T1 cells. First, 4T1 cells (1×10^5 cells/well) were plated in a 12-well plate slide and maintained for 12 h. Then, fresh media containing the Phy-Mast-M and vector were exchanged for another 1 h, 3 h, and 6 h of culture. Next, 4T1 cells were washed twice with PBS and fixed with 4% formaldehyde for 15 min at room temperature. The cells were counterstained with JC-1 (C2006, Beyotime, China) to assess the mitochondrial membrane. Coverslips were mounted on glass microscope slides with a drop of anti-fade mounting media to reduce fluorescence photobleaching. The condition of the mitochondrial membrane was visualized using the Leica DM2700 Portho fluorescence microscope (Leica Microsystems, Wetzlar, Germany).

Cell Clone

Cells were inoculated at a concentration of 500 cells per well into a 6-well plate for incubation. Then, fresh media containing Phy-Mast-M were exchanged for another 7 days of culture. Subsequently, cells were fixed with a fixative and stained with crystal violet.

Cell Cycle Analysis

4T1 cells (2×10^5 cells/well) were seeded into a 6-well plate and initially for 12 h. They were then treated with Mast-M, Phy-Mast-M and doxorubicin further incubated for 24 h. Cells were harvested and fixed overnight in 70% ethanol at −20°C. Then, the solution containing cultured cells was centrifuged at 800 rpm for 5 min, the supernatant was discarded, and 1 mL PBS was added. The solution was resuspended and allowed to rest at room temperature for 15 min. The solution was centrifuged again and the supernatant was discarded. Then, samples were incubated in a solution containing 10 mg/mL RNase and 1 mg/mL PI (Yeasen Biotech) at 37°C for 30 min in the dark. The DNA content was determined using flow cytometry (Becton, Dickinson &Co).

Subcutaneous Mouse Model

BALB/c mice (aged 6 to 8 weeks) were subcutaneously injected with 1×10^7 4T1 cells on the right side of the lower limb. Tumor-bearing mouse were assigned randomly into the following three experimental groups: 1. PBS group (injected with PBS); 2. Mast-M group (injected with 2.7 mg/kg Mast-M); 3. Phy-Mast-M group (injected with 2.7 mg/kg Phy-Mast-M). The treatment begins when the tumor volume reaches approximately 50–75 mm^3. The drug is injected intravenously every four days, for a total of four doses and the first dose is given on day 0 and recorded. From this point onwards, the weight and tumor volume of the mice are carefully measured every two days. Tumor volume is calculated using an established formula: length × (width)^2 × 0.52. The mice were euthanized on day 20, and the heart, liver, spleen, lung, and kidney tissues of tumor-bearing mice were harvested for histological examination through hematoxylin and eosin (H&E) staining. Additionally, the tumor tissue underwent staining procedures for H&E, Ki-67, Bcl-2, and TUNEL markers to evaluate specific cellular characteristics and molecular markers associated with tumorigenesis.

Fluorescence Imaging

The 4T1 tumor-bearing mice (volume 50–75 mm^3) were randomly divided into two groups (n= 6) and injected intravenously with Phy-Mast-M-ICG / Mast-M-ICG (Contains the same amount of ICG, 1.0 mg/kg). Animals were given isoflurane (RWD Life Science) for anesthesia, and fluorescence signals were assessed with the small animal imaging systems (Series III 900/1700) at 1, 3, 6, 12, 24, 36, 48, and 72 h. To further observe nanoprobe biodistribution in vivo, mouse organs were dissected for fluorescence imaging at 48 h post-injection.

Safety Study

The biosafety of Phy-Mast-M was assessed in healthy BALB/c mice. After injection with Phy-Mast-M, Mast-M (2.7 mg/kg) and PBS was continuously injected once a day for 4 days. After 48 h, blood samples were collected for testing blood routine and biochemical indexes, including alanine aminotransferase (ALT), aspartate aminotransferase (AST), creatinine (Cre), and blood urea nitrogen (Urea).

Statistical Analysis

The data are presented as the mean values ± standard deviations. Statistical significance was determined using two-way analysis of variance. Graphs and figures were generated using GraphPad Prism software. Fluorescence images and immunohistochemical images were processed and statistically analysed using ImageJ software. For the reported data, the symbol "*" denotes $P < 0.05$, "**" denotes $P < 0.01$, "***" denotes $P < 0.001$, "****" denotes $P < 0.0001$, and "ns" indicates no statistically significant difference. All statistically analysed data included a minimum of 3 samples.

Results

Synthesis and Characterization of Phy-Mast-M

Mast-M is an active substance and natural polypeptide. It is composed of amino acids as its basic unit (Figure S1). Phy-Mast-M was prepared by simply mixing Mast-M with SPC (Figure 1A). General characterization results showed that Phy-Mast-M is a milky, transparent, clarified liquid (Figure S2). TEM images showed that Phy-Mast -M was monodispersed and spherical, and DLS analysis indicated an average hydrated particle size of 125.67 ± 45.79 nm (Figure 1B and C). A zeta potential value of +32.05 ± 17.27 mV was observed for Phy-Mast-M (Figure 1D), indicating its potential to easily attach to the surface of cancer cells and exhibit pharmacological effects. Figure 1E showed that the mixture of SPC and Mast-M was insoluble in dichloromethane, but Phy-Mast -M did not solidify or form flocculent precipitates in dichloromethane. These results indicate that Phy-Mast-M is not a simple physical mixture of SPC and Mast-M, but a complex formed by weak interactions (electrostatic, hydrophobic, hydrogen bonding, van der Waals forces, etc). (Figure S3). The results of HPLC and FTIR analysis further demonstrate the successful combination of Mast-M with SPC (Figure 1F and G).

No precipitation or flocculation occurred in our Phy-Mast-M complex during 48 h of general monitoring. Moreover, even after 48 hours of standing followed by laser irradiation, the dispersion remained visually favorable, as depicted in Figure 1H, highlighting the complex's remarkable stability. HPLC content monitoring over 28 days further confirmed the stability of the compound (Figure S4). Besides, to further verify its stability in vitro, the probe was dissolved in different media (PBS, water, 10% FBS, and DMEM cell culture medium) and the particle size was measured at different times. We found that the particle size of Phy-Mast-M did not change significantly at 0, 6, 12, 24, and 48 h (Figure 1I). Overall, the small particle size, monodisperse size distribution, and high zeta potential indicated the excellent stability of Phy-Mast-M.

In vitro Cytotoxicity of Phy-Mast-M

As shown in Figure 2A, significantly decreased cell viability was observed upon treatment with Phy-Mast-M after a 24-h incubation period, when compared with untreated cells and the Mast-M group, suggesting its excellent cytotoxic effects on 4T1 cells. The results of the CCK-8 assay conducted using MDA-MB-231 cells also corroborated the experimental conclusions (Figure 2B). Furthermore, the IC50 curves of Mast-M and Phy-Mast -M can also intuitively convey this experimental result (Figure 2C). Notably, Phy-Mast-M has been observed to exert a broad cytotoxic effect on various cancer cell lines, including BT-549, HeLa, CT-26, HepG2, and HT-29, as demonstrated in Figure S5. Furthermore, Phy-Mast-M has been demonstrated to exhibit low toxicity to normal breast epithelial cells MCF-10A, with a slightly stronger effect compared to the Mast-M group. This increased cytotoxicity may be attributed to the enhanced cellular uptake observed for Phy-Mast-M.

Cellular Uptake and Colocalization of Phy-Mast-M

As shown in (Figure 2D), the uptake of drugs by 4T1 cells gradually increased with the prolongation of drug incubation time. Notably, the uptake of FITC-Phy-Mast-M by 4T1 cells was more substantial than that of FITC-Mast-M. The mean fluorescence quantization map of FITC also shows the same experimental results. This is attributable to lecithin being a basic component of the cell membrane and having a strong affinity with it. When Mast-M forms a phospholipid complex with lecithin, the latter, acting as a drug carrier, can promote the entry of the substance from the cell membrane into the cell. In order to further explore the anti-tumor mechanism of Phy-Mast-M,

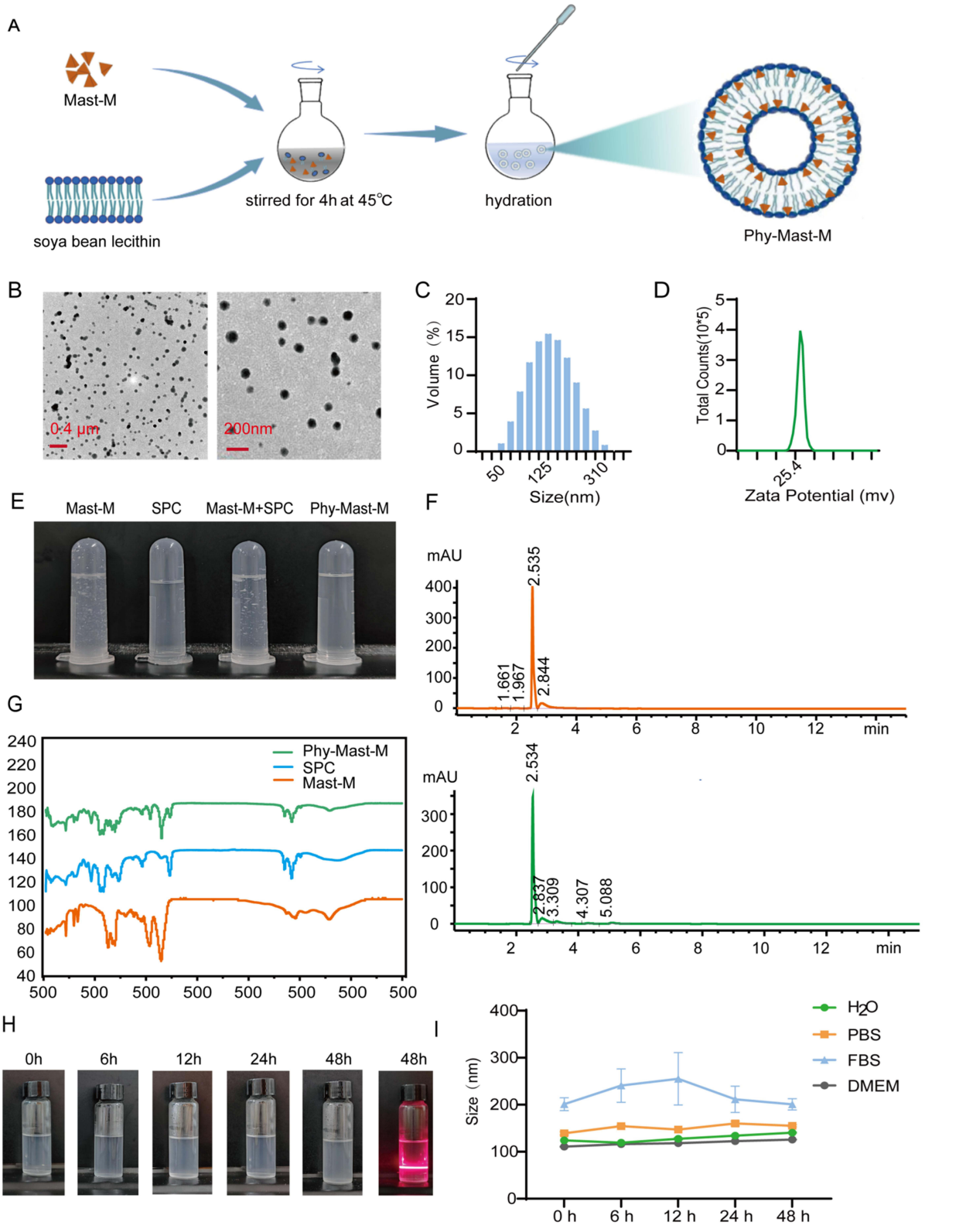

Figure 1 Synthesis and characterization of Phy-Mast-M. (**A**). Preparation of Phy-Mast-M. (**B**). Transmission electron microscope (TEM) images of Phy-Mast-M. (**C**). The size of Phy-Mast-M. (**D**). The zeta potential value of Phy-Mast-M. (**E**). Solubility of Mast-M, SPC, Mast-M+SPC, and Phy-Mast-M in methylene chloride solvent. (**F**). HPLC Test results for Mast-M (top) and Phy-Mast-M (bottom), the FTIR (**G**) of SPC, SPC+Mast-M, and Phy-Mast-M. (**H**). Physical properties and laser detection of Phy-Mast-M at 0 h, 6 h, 12 h,24 h, and 48 h. (**I**). The stabilities and size of Phy-Mast-M in different media (PBS, 10% fetal bovine serum (FBS), water, and DMEM cell culture medium). At 0, 6, 12, 24, and 48 h, the hydrodynamic diameters were measured for the corresponding solutions (n= 3).

https://doi.org/10.2147/IJN.S481871

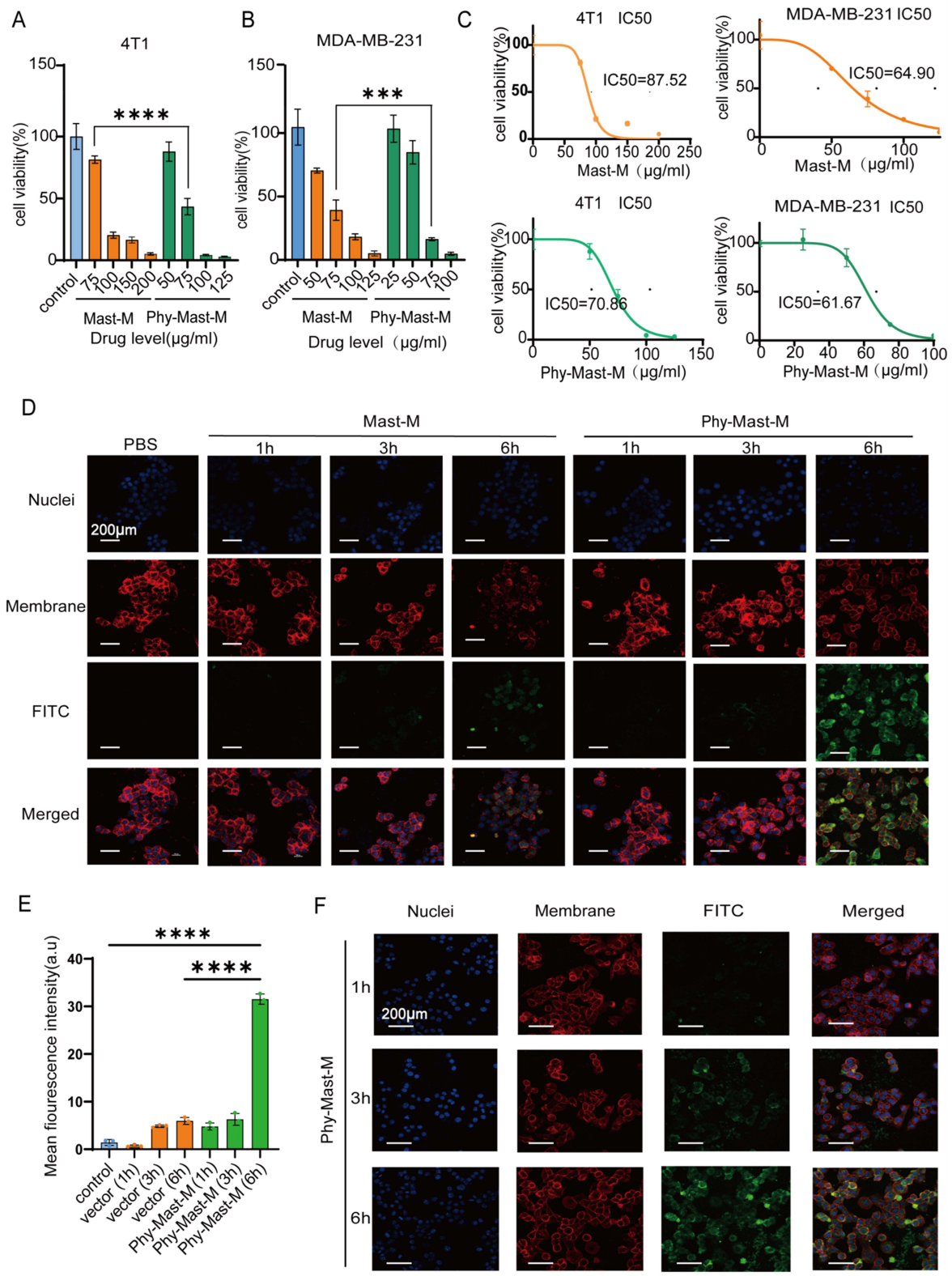

Figure 2 Anti-tumor activity and cytoendocytosis of Phy-Mast-Md. (**A**). Cytotoxicity detection for 4T1 cells using Phy-Mast-Md and Mast-M. (n= 6, ****p< 0.0001) (**B**). Cytotoxicity detection for MDA-MB-231 cells using Phy-Mast-Md and Mast-M. (n= 6, ***p< 0.001) (**C**). Using Phy-Mast-M and Mast-M to derive the IC50 statistics of 4T1 cells (left) and 231 cells (right). (**D**). Absorption of Mast-M and Phy-Mast-Md by 4T1 cells at 1, 3, and 6 h. Confocal photography (red: Dil cell membrane staining, blue: DAPI cell nucleus staining, green: FITC drug label fluorescence). (**E**). Statistical diagram showing the average fluorescence intensity of FITC. (n= 3, ****p<0.0001) (**F**). Phy-Mast-M enters 4T1 cells to facilitate colocalization confocal photography.

the cell colocalization of the complex was detected. As shown in Figure 2F, most of the drug enters the cytoplasm, and a small part enters the nucleus.

Phy-Mast-M Induces Apoptosis by Destroying the Mitochondrial Membrane in vitro

Due to the large amounts of drugs entering the cytoplasm, we hypothesized that the complex would promote cancer cell apoptosis by destroying mitochondrial membranes. Therefore, we performed flow cytometry-based detection of the complex to assess whether apoptosis was promoted and performed confocal imaging to assess mitochondrial membrane staining. Apoptosis of 4T1 cells was then evaluated after transfection with different formulations, and cells were analyzed to detect cell apoptosis after staining them with Annexin-V-FITC and PI (Figure 3A). It was demonstrated that the carrier drug group did not induce apoptosis, while Mast-M and Phy-Mast-M both induced 4T1 cell apoptosis. However, it is noteworthy that the pro-apoptotic ability of the Phy-Mast-M drug group was notably stronger than that of the Mast-M drug group. The quantization graph (Figure 3B) confirms these findings.

To further validate the ability of Phy-Mast-M to promote apoptosis in tumor cells, we conducted Western Blot (WB) analysis to detect the expression of relevant apoptotic factors. As shown in Figure S6, Phy-Mast-M upregulated the expression of Bax and caspase-3, and this upregulation is positively correlated with concentration. These results suggest that Phy-Mast-M can promote apoptosis in tumor cells, which was consistent with the flow cytometry data.

As shown in (Figure 3C and D), the mitochondrial membrane potential of the drug carrier group was similar to that of the control group, with both groups yielding robust red fluorescence signals. This observation suggests that the drug carrier does not induce significant damage to the cellular mitochondrial membrane. In contrast, the fluorescence characteristics of the Phy-Mast-M drug group evolved gradually over time, showing a progressive attenuation of red fluorescence and a concomitant increase in green fluorescence intensity. This demonstrated that Phy-Mast-M can disturb the mitochondrial membrane of tumor cells.

Phy-Mast-M Affects Cell Cloning and Proliferation

Experimental findings pertaining to cell proliferation indicate that Phy-Mast-M had a notable impact on 4T1 (Figure 3E and F) and MDA-MB-231 cells (Figure S7A and B). Subsequent flow cytometry analysis revealed that Phy-Mast-M influenced the cell cycle of 4T1 cells, resulting in the inhibition of clonal proliferation among cancer cells (Figure 3G). These results underscore the potential of Phy-Mast-M as a candidate for impeding cancer cell growth and warrant further investigation into its therapeutic applications.

Phy-Mast-M Fluorescence Imaging and Biodistribution

To further confirm the tumor targeting specificity of Phy-Mast-M in vivo, 4T1-tumor-bearing mice were intravenously injected with Phy-Mast-M-ICG and free Mast-M-ICG. Fluorescence imaging analysis consistently detected a robust signal in the tumors of mice treated with Phy-Mast-M-ICG, whereas only a faint signal was evident in the tumor region in the free Mast-M-treated group over the same period. In contrast, the Phy-Mast-M-ICG group showed a strong fluorescence signal in the tumor, and the signal intensity was retained for up to 72 h post-injection (Figure 4A and B). To investigate the biodistribution of Phy-Mast-M in vivo, mouse organs were dissected for fluorescence imaging at 48 h post-injection, as illustrated in Figure 4C. Clearly, the tumors of the Phy-Mast-M group showed more intense mean fluorescence signals than the Mast-M group (Figure 4C and D). These results provide compelling evidence that Phy-Mast -M enhances the bioavailability and tumor targeting of Mast-M.

In vivo Anti-Tumor Studies

Next, we assessed the in vivo anti-tumor efficacy of Phy-Mast-M on breast tumors. BALB/c mice, inoculated with 4T1 cells via hypodermic injection, were treated with four administrations once the tumor volume reached approximately 50–75 mm^3 (Figure 4E). As depicted in Figure 4F, no significant variations in body weight were observed across all treatment groups, indicating that Phy-Mast-M exhibits a favorable safety profile. Analysis of tumor volumes revealed that the Phy-Mast-M group demonstrated superior tumor suppression compared to the PBS and Mast-M groups (Figure 4G and H). Additionally, mice images in Figure S8 clearly support this outcome. Furthermore, the statistical results of tumor

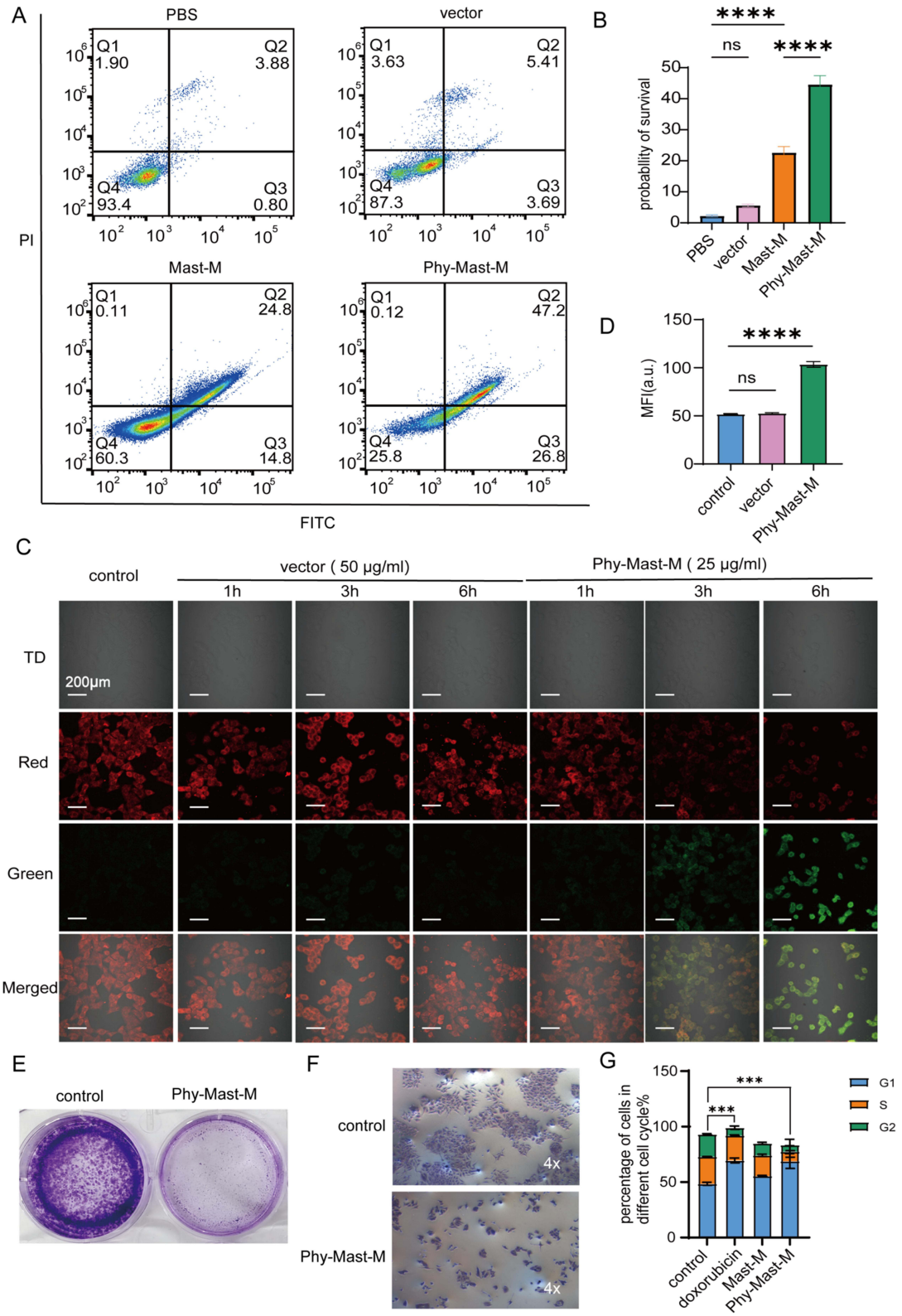

Figure 3 Phy-Mast-Md promotes apoptosis by destroying the mitochondrial membrane. (**A**). Apoptotic flow detection of Phy-Mast-M. (**B**). Quantitative statistics of streaming data (n= 3, ****p<0.0001). (**C**). Mitochondrial membrane potential detection at 1, 3, and 6 h after the administration of vector and Phy-Mast-Md (red, mitochondrial membrane is normal; green, mitochondrial membrane is damaged). (**D**). Bar chart of green fluorescence intensity of various drug groups 6 h after cell treatment (n= 3, ****p<0.0001). (**E** and **F**). Cloning and proliferation of 4T1 cells. (**G**) Cell cycle detection of 4T1 cells (n= 3, ***p<0.001, the p-values represent G1 region in each group compared with G1 region of control group).

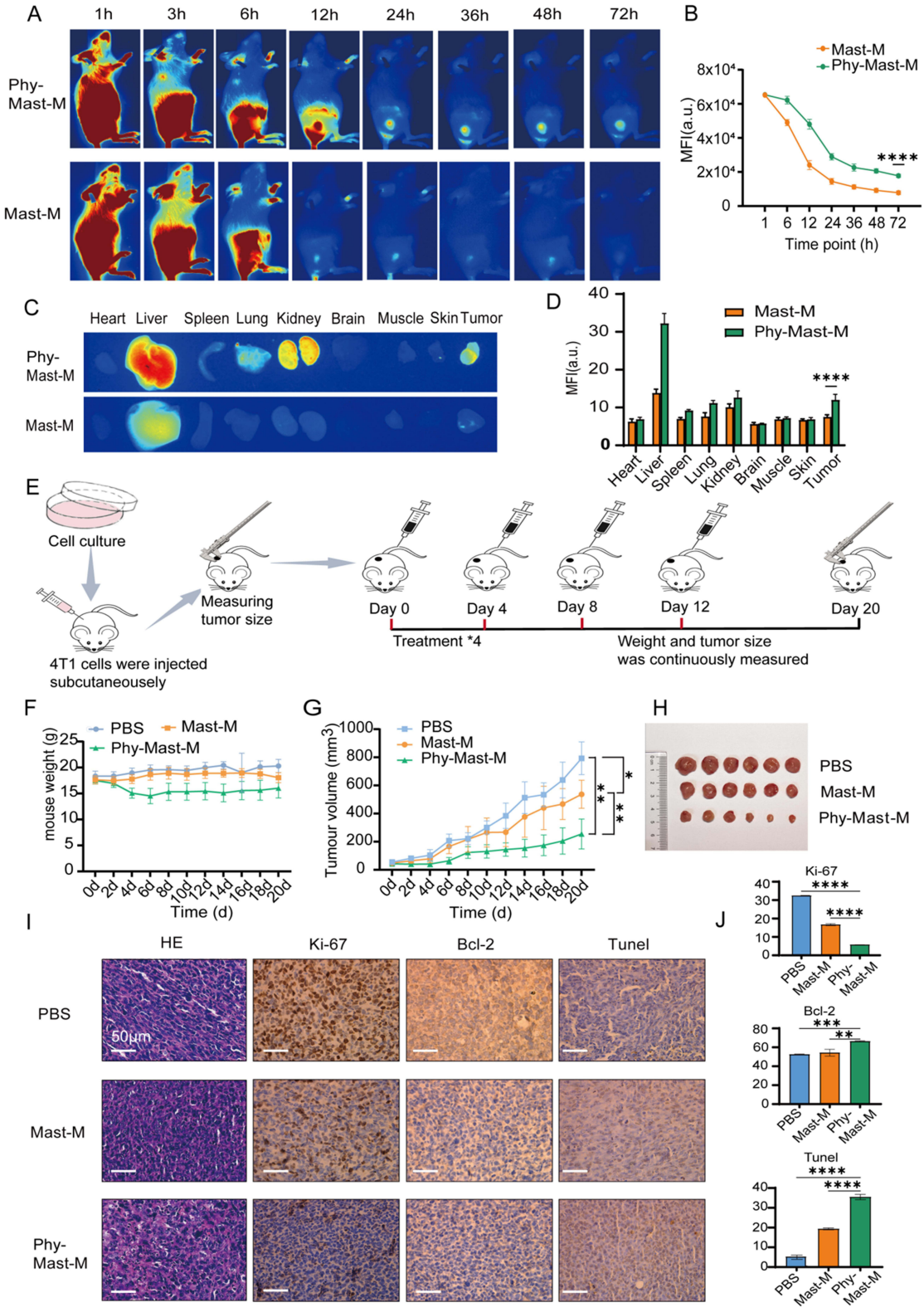

Figure 4 In vivo anti-tumor studies of fluorescence imaging and biodistribution of Phy-Mast-M. (**A**). Fluorescence imaging of mice at 1, 3, 6, 12, 24, 36, 48, and 72 h after administration. (**B**). Quantification of average fluorescence intensity during fluorescence imaging (n= 6, ****p<0.0001). (**C**). Fluorescence imaging of various tissues of mice in different drug groups. (**D**). Quantitative map of average fluorescence intensity in each tissue during fluorescence imaging g(n= 6, ****p<0.0001). (**E**). The modeling process of subcutaneous tumors in mice. (**F**). Weight monitoring of mice (n= 6). (**G**). Tumor size monitoring of mice (n= 6, *p<0.05, **p<0.01). (**H**). Visual map of tumor size of each drug group. (**I**). HE staining and KI-67, Bcl-2, and TUNEL staining of tumor tissue. (**J**). Quantitative map of tumor tissue staining (n= 3, **p<0.01, ***p<0.001, ****p<0.0001).

https://doi.org/10.2147/IJN.S481871

Table 1 Statistical Results for the Tumor Inhibition Rate. (N= 6)

Tumor growth inhibition rate		
PBS	722.43±194.33	
Mast-M	613.511±138.29	15.07%
Phy-Mast-M	202.05±139.91	72.03%

inhibition rates show that Phy-Mast-M achieved a tumor inhibition rate of 72.03%, significantly exceeding that of the Mast-M group (Table 1). These findings suggest that Phy-Mast-M possesses potent in vivo antitumor effects, outperforming the free Mast-M group. In addition, to further substantiate the in vivo evidence that Phy-Mast-M exerts antitumor effects by promoting apoptosis, immunohistochemical staining was conducted on tumor tissues. The staining results confirmed an increase in the apoptotic markers Bcl-2 and TUNEL, along with a decrease in Ki-67, indicating a substantial induction of tumor cell apoptosis in the Phy-Mast-M group (Figure 4I and J). These findings suggest that Phy-Mast-M can elicit therapeutic effects on tumors by facilitating cellular apoptosis.

Safety of Use of Phy-Mast-M

We further collected the heart, liver, spleen, lung, and kidney of tumor model mice to perform H&E staining. No significant histopathological changes, including necrosis, inflammation, or structural destruction were observed in organs obtained from the Phy-Mast-M group (Figure 5A). Furthermore, the hematological analysis revealed that all blood routine indices for the Phy-Mast-M group were within the normal parameters (Figure 5B). In addition, blood biochemistry indicators were largely unaltered, except for a slight decrease in urea levels, which showed a slight decrease compared to the normal range. Nonetheless, when compared to the normal group, there was no significant difference in urea levels, which were still comparable to the normal range and might be attributed to reduced sample capacity (Figure 5C). Collectively, these findings indicate that Phy-Mast-M is safe for in vivo administration.

Discussion

Mast-M, a small molecule peptide with anti-tumor active substances, was extracted and isolated by our team from Yunnan Dehong *Vespa magnifica*.[10,12] It has great potential for the development of new anti-tumor drugs and is expected to solve the problem of shortage of certain new anti-tumor drugs in clinical settings. In the present study, a novel anti-tumor complex, Phy-Mast-M, was developed using a solvent evaporation method. This formulation exhibits enhanced characteristics, including a smaller size, lower size distribution, higher zeta potential, and better stability. Moreover, it could induce apoptosis in cancer cells by destroying the mitochondrial membrane and arresting the cell growth cycle, thus achieving an anti-tumor effect for the first time. As expected, in the 4T1 tumor-bearing mouse model, this innovative strategy resulted in excellent anti-tumor effects.

As an active substance and natural polypeptide, Mast-M has a mode of action that is similar to that of biological agents such as antibodies and therapeutic proteins, but these peptides have lower immunogenicity and are cheaper to produce because they can be synthesized chemically.[21–23] We found that Mast-M exhibits cytotoxic effects against tumors in vitro.[10] However, the anti-tumor mechanism of Mast-M is still unclear and has not been investigated in anti-tumor therapy research. Previous studies have confirmed that other bee toxins such as melittin and apamin can disrupting cell membrane stability,[24,25] affecting cell metabolism,[26,27] inhibit the growth of tumor cells via apoptosis promotion, cell cycle inhibition,[28,29] signaling cascade regulation,[30] and other mechanisms.[31,32] We speculate that its mechanism of action may be similar to that of bee venom, but there are certain differences. The anti-tumor mechanism has remained unexplored for Mast-M. Heren, the anti-tumor mechanism of wasp toxin Mast-M was initial investigated in this study. The results showed that Phy-Mast-M could inhibit tumor cells via various avenues, promote apoptosis in tumor cells by destroying mitochondrial membranes of cells, or hinder the growth cycle of tumor cells. Therefore, a deeper understanding of the anti-tumor molecular mechanisms of Mast-M still requires further exploration, and our research group continues to delve into this area. Overall, multi-pathway anti-tumor mechanisms can reduce drug resistance occurrence

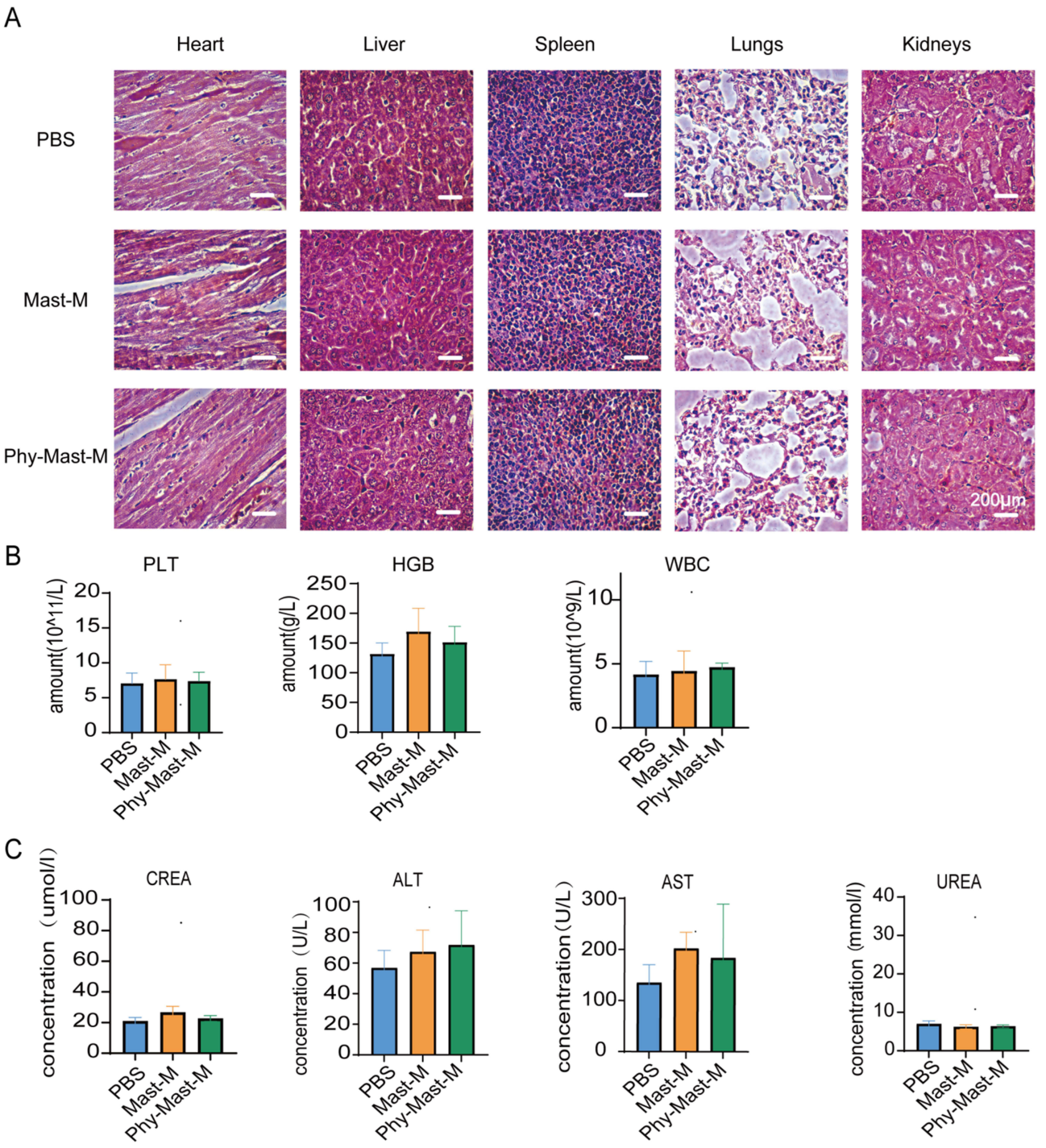

Figure 5 Safety of Phy-Mast-M. (**A**). HE staining of tumor-bearing mice after drug treatment. (**B**). Blood routine tests in mice. (**C**). Blood biochemical detection in mice. (n= 3).

and development. This provides guidance for the discovery of novel strategies and the development of new drugs for cancer treatment.

We found that Mast-M exhibits cytotoxicity in vitro. However, its application in cancer treatment is limited because of its rapid metabolism and short blood circulation time, which makes it challenging for Mast-M to accumulate effectively in tumor sites.[10–13] Therefore, improving the biological distribution characteristics of Mast-M in vivo is necessary to achieve a lower toxicity and substantial anti-tumor effect. Modifying the delivery method is the most

https://doi.org/10.2147/IJN.S481871

prevalent and effective strategy to address this issue. Currently, the phytosome serves as a molecular drug delivery vehicle, characterized as a hybrid nanoparticle that entraps the drug within SPC.[33,34] It mimics the lipid-soluble and water-soluble properties of SPC and is largely amphipathic. This characteristic facilitates its transport from the surrounding water-soluble environment to the lipid-soluble environment of the cancer cell membrane, enhancing its effectiveness. Thus, phytosome technology substantially improves bioavailability, enhances efficacy, and reduces drug toxicity, providing a fundamental advantage and breakthrough for the clinical application of some drugs.[20] A safe and effective phytosome phospholipid complex design has increasingly attracted more and more attention in recent years as it is essential for phytosome formation. The daidzein-phospholipid complex, salvianolic acid B-phospholipid complex, clarithromycin-phospholipid complex, and other liposome delivery systems reportedly have unique advantages due to their excellent biocompatibility and membrane fusion properties.[20,35,36] In this study, we selected Mast-M as the active anti-tumor substance and adopted biocompatible liposome nanomaterials as the main delivery system to synthesize a new liposome nanomedicine using the solvent evaporation method. The results showed that Phy-Mast-M exhibited better biological distribution, blood cycle duration, and anti-tumor efficacy than Mast-M, both in vivo and in vitro. Phy-Mast-M shows excellent safety and clinical translational potential, providing more drug choices for the treatment of breast cancer.

Several limitations are associated with the present study. Primarily, the anti-tumor molecular mechanism of Mast-M has not been thoroughly understood. Though our study demonstrated the ability of Mast-M to promote apoptosis and induce cell cycle arrest within cancer cells, Mast-M may potentially have tumoricidal effects as it modulates the tumor microenvironment, enhances immune regulation, and engages with other unidentified mechanisms. Therefore, it is necessary to explore the anti-tumor mechanism of Mast-M further in the future. Moreover, in the present study, Phy-Mast-M was only targeted to the tumor site because of the EPR effect; it lacks specific targeting capabilities. To enhance the efficacy of targeted breast cancer treatment, additional modifications to enhance liposome targeting are necessary.

Conclusion

In conclusion, our results suggest that Phy-Mast-M has the potential to deliver efficient and safe treatment for breast cancer. This has significant implications for the development of novel anti-tumor therapeutics and could facilitate the development of safe and efficient new anticancer nanomedicines to effectively control local tumors. Such advancements not only have promising clinical utility for enhancing the survival rates and quality of life of cancer patients but also have practical implications for the mitigation of societal costs associated with cancer treatment.

CRediT Authorship Contribution Statement

All authors made a significant contribution to the work reported, whether that is in the conception, study design, execution, acquisition of data, analysis and interpretation, or in all these areas; took part in drafting, revising or critically reviewing the article; gave final approval of the version to be published; have agreed on the journal to which the article has been submitted; and agree to be accountable for all aspects of the work.

Data Sharing Statement

Data will be made available upon reasonable request to the corresponding author.

Acknowledgments

This work was supported by the Natural Science Foundation of Fujian Province of China (Grant No.2023J05273), Fujian Provincial Health Commission science and technology plan project youth research project (Grant No.2022QNB012), Xiamen Natural Science Foundation of China (Grant No.3502Z202372071) and Yunnan Fundamental Research Projects (Grant No.202401AS070029).

Disclosure

All authors have none conflicts to declare.

References

1. Liang Y, Liu J, Zhao C, et al. HER2-targeting two-dimensional black phosphorus as a nanoplatform for chemo-photothermal therapy in breast cancer. *Mater Today Bio*. 2023;23:100812. doi:10.1016/j.mtbio.2023.100812
2. Nedeljković M, Damjanović A. Mechanisms of chemotherapy resistance in triple-negative breast cancer—how we can rise to the challenge. *Cells*. 2019;8(9):957. doi:10.3390/cells8090957
3. Yin L, Duan JJ, Bian XW, et al. Triple-negative breast cancer molecular subtyping** and treatment progress. *Breast Cancer Res*. 2020;22:1–13. doi:10.1186/s13058-020-01296-5
4. Yang RQ, Wang PY, Lou KL, et al. Biodegradable Nanoprobe for NIR-II Fluorescence Image-Guided Surgery and Enhanced Breast Cancer Radiotherapy Efficacy. *Adv Sci*. 2022;9(12):2104728. doi:10.1002/advs.202104728
5. Li W, Xu M, Li Y, et al. Comprehensive analysis of the association between tumor glycolysis and immune/inflammation function in breast cancer. *J Transl Med*. 2020;18:1–12. doi:10.1186/s12967-020-02267-2
6. Wu D, Si M, Y XH, et al. Nanomedicine applications in the treatment of breast cancer: current state of the art. *Int j Nanomed*. 2017;12:5879–5892. doi:10.2147/IJN.S123437
7. Lee JA, Son MJ, Choi J, et al. Bee venom acupuncture for rheumatoid arthritis: a systematic review of randomised clinical trials. *BMJ open*. 2014;4 (11):e006140. doi:10.1136/bmjopen-2014-006140
8. Lee JD, Park HJ, Chae Y, et al. An overview of bee venom acupuncture in the treatment of arthritis. *Evidence-Based Comple Altern Med*. 2005;2 (1):79–84. doi:10.1093/ecam/neh070
9. Xu X, Li J, Lu Q, et al. Two families of antimicrobial peptides from wasp (Vespa magnifica) venom. *Toxicon*. 2006;47(2):249–253. doi:10.1016/j.toxicon.2005.10.015
10. Si-tong Z, Yi-hao C, Lian-li N, et al. Determination of peptide and protein diversity in venom of Vespa magnifica (Smith) on structure and function. *Nat Prod Res Dev*. 2019;31:1596–1601.
11. Gao Y, Yu WX, Duan XM, et al. Wasp venom possesses potential therapeutic effect in experimental models of rheumatoid arthritis. *Evidence-Based Comple Alternative Med*. 2020;2020(1):6394625. doi:10.1155/2020/6394625
12. Wang M, Wu XM, He M, et al. Mastoparan M extracted from Vespa magnifica alleviates neuronal death in global cerebral ischemia-reperfusion rat model. *Iran J Basic Med Sci*. 2022;25(3):320. doi:10.22038/IJBMS.2022.60745.13461
13. Zhao H, Wang M, Gao Y, et al. Vespakinin-M, a natural peptide from Vespa magnifica, promotes functional recovery in stroke mice. *Commun Biol*. 2022;5(1):74. doi:10.1038/s42003-022-03024-5
14. Zhu Y, Wang A, Zhang S, et al. Paclitaxel-loaded ginsenoside Rg3 liposomes for drug-resistant cancer therapy by dual targeting of the tumor microenvironment and cancer cells. *J Adv Res*. 2023;49:159–173. doi:10.1016/j.jare.2022.09.007
15. Zhang XQ, Xu X, Bertrand N, et al. Interactions of nanomaterials and biological systems: implications to personalized nanomedicine. *Adv Drug Delivery Rev*. 2012;64(13):1363–1384. doi:10.1016/j.addr.2012.08.005
16. Neubi GMN, Opoku-Damoah Y, Gu X, et al. Bio-inspired drug delivery systems: an emerging platform for targeted cancer therapy. *Biomater Sci*. 2018;6(5):958–973. doi:10.1039/C8BM00175H
17. Filipczak N, Pan J, Yalamarty SSK, et al. Recent advancements in liposome technology. *Adv. Drug Delivery Rev*. 2020;156:4–22. doi:10.1016/j.addr.2020.06.022
18. Ahmed KS, Hussein SA, Ali AH, et al. Liposome: composition, characterisation, preparation, and recent innovation in clinical applications. *J Drug Targeting*. 2019;27(7):742–761. doi:10.1080/1061186X.2018.1527337
19. Fetterly GJ, Straubinger RM. Pharmacokinetics of paclitaxel-containing liposomes in rats. *Aaps Pharmsci*. 2003;5:90–100. doi:10.1208/ps050432
20. Hou Z, Li Y, Huang Y, et al. Phytosomes loaded with mitomycin C–soybean phosphatidylcholine complex developed for drug delivery. *Mol Pharmaceut*. 2013;10(1):90–101. doi:10.1021/mp300489p
21. Vlieghe P, Lisowski V, Martinez J, et al. Synthetic therapeutic peptides: science and market. *Drug Discovery Today*. 2010;15(1–2):40–56. doi:10.1016/j.drudis.2009.10.009
22. Skwarczynski M, Toth I. Peptide-based synthetic vaccines. *Chem Sci*. 2016;7(2):842–854. doi:10.1039/C5SC03892H
23. Sudhina S, Heera S, Mohan A, et al. Self-assembled smart nanostructures for drug delivery applications[M]//Nanostructured Materials for Biomedical Applications. *Elsevier*. 2024;229–279.
24. Adade CM, Oliveira IR, Pais JA, et al. Melittin peptide kills Trypanosoma cruzi parasites by inducing different cell death pathways. *Toxicon*. 2013;69:227–239. doi:10.1016/j.toxicon.2013.03.011
25. Kroemer G. Introduction: mitochondrial control of apoptosis. *Biochimie*. 2002;84(2–3):103–104. doi:10.1016/S0300-9084(02)01382-2
26. Park HJ, Lee SH, Son DJ, et al. Antiarthritic effect of bee venom: inhibition of inflammation mediator generation by suppression of NF-kappaB through interaction with the p50 subunit. *Arthritis Rheum*. 2004;50(11):3504–3515. doi:10.1002/art.20626
27. Park JH, Jeong YJ, Park KK, et al. Melittin suppresses PMA-induced tumor cell invasion by inhibiting NF-kappaB and AP-1-dependent MMP-9 expression. *Mol Cells*. 2010;29(2):209–15.31. doi:10.1007/s10059-010-0028-9
28. Pandey P, Khan F, A KM, et al. An updated review summarizing the anticancer efficacy of melittin from bee venom in several models of human cancers. *Nutrients*. 2023;15(14):3111. doi:10.3390/nu15143111
29. Shi P, Xie S, Yang J, et al. Pharmacological effects and mechanisms of bee venom and its main components: recent progress and perspective. *Front Pharmacol*. 2022;13:1001553. doi:10.3389/fphar.2022.1001553
30. Stuhlmeier KM. Apis mellifera venom and melittin block neither NF-kappa B-p50-DNA interactions nor the activation of NF-kappa B, instead they activate the transcription of proinflammatory genes and the release of reactive oxygen intermediates. *J Immunol*. 2007;179(1):655–664. doi:10.4049/jimmunol.179.1.655
31. Peric S Koglin DYM, Kaymakanov N, Koglin S, et al. Honey bee (Apis mellifera) venom induces AIM 2 inflammasome activation in human keratinocytes. *Allergy*. 2012;67(11):1400–1407. doi:10.1111/all.12022
32. Palm NW, Medzhitov R. Role of the inflammasome in defense against venoms. *Proc Natl Acad Sci U S A*. 2013;110(5):1809–1814. doi:10.1073/pnas.1221476110
33. Xiang H, Shen B, Zhang C, et al. Bioactive Nanoliposomes for Enhanced Sonodynamic-Triggered Disulfidptosis-Like Cancer Cell Death via Lipid Peroxidation. *Int j Nanomed*. 2024. 8929–8947. doi:10.2147/IJN.S464178

34. Shaji SG, Patel P, Mamani UF, et al. Delivery of a STING Agonist Using Lipid Nanoparticles Inhibits Pancreatic Cancer Growth. *Int j Nanomed*. 2024;Volume 19:8769–8778. doi:10.2147/IJN.S462213
35. Ma Y, Zhao X, Li J, et al. The comparison of different daidzein-PLGA nanoparticles in increasing its oral bioavailability. *Int j Nanomed*. 2012;7:559–570. doi:10.2147/IJN.S27641
36. Liu W, Zhou Z, Zhu L, et al. Chemopreventive efficacy of salvianolic acid B phospholipid complex loaded nanoparticles against experimental oral carcinogenesis: implication of sustained drug release. *Ann translat Med*. 2022;10(5).